JOURNAL OF SPACECRAFT AND ROCKETS
Vol. 42, No. 1, January–February 2005

Pulsed Plasma Thruster System for Microsatellites

Christopher D. Rayburn,* Mark E. Campbell,† and A. Thomas Mattick‡
University of Washington, Seattle, Washington 98104

The design and qualification of a pulsed plasma thruster (PPT) system for microsatellites is presented. Developed for the University of Washington's Dawgstar satellite, the micro-PPT provides formation keeping, orbit maintenance, and attitude control functions for satellites in the 10–100-kg range. Thrust is created when solid Teflon® propellant is ionized by a pulsed, high-current electrical arc and accelerated by a combination of electromagnetic and gas dynamic forces. The system presented provides thrust levels from 60 to 275 μN with specific impulses up to 266 s. A centralized power-processing unit utilizing high voltage switching enables a reduction in system mass when compared to previous designs. The total mass for the system presented is 4.20 kg, which enables control of three axes of rotation and two axes of translation. Approximately 1.7 million pulses were successfully accumulated on the flight qualification unit, representing a total system impulse of approximately 1000 N · s. Mission design, mechanical and electrical design, and detailed results from ground testing are discussed.

Nomenclature

A	=	fuelbar surface area
A_R	=	fuelbar aspect ratio
B	=	magnetic field strength
C	=	discharge circuit capacitance
E	=	discharge energy
F_{instant}	=	instantaneous force on the thruster
f	=	firing frequency
I_{bit}	=	impulse bit
I_{sp}	=	specific impulse
i	=	discharge current
L	=	discharge circuit inductance
l	=	length of electrodes
m_D	=	mass ablated per discharge
P	=	power
R	=	discharge circuit resistance
T_{gas}	=	thrust from gas-dynamic expansion
T_{magnetic}	=	thrust from magnetic forces
t	=	time
V_0	=	initial discharge voltage
γ	=	ratio of specific heats
μ	=	magnetic permeability

Introduction

THE use of multiple satellite clusters, coordinated together as a single virtual satellite, is an important focus area of the Earth and space science, defense, and commercial industries. In the U.S. Department of Defense there is growing interest for highly maneuverable satellites that would be able to perform on-orbit servicing and space-based surveillance. Eventually it is conceived that these missions would be completed with fleets of microsatellites either independently or in constellations.[1,2] NASA's Origins program is designing a series of spaceborne interferometry missions that will examine far off planets for possible life forms. Mission requirements range from two to eight satellites that will require nanometer-level optical positioning (centimeter-level spacecraft positioning).[3] There are also planned Earth science constellation missions to allow more detailed mapping of the Earth's magnetosphere and even commercial ventures that have focused on using distributed satellite technology.[4] The common theme between these systems is increased performance and reliability at a decreased cost.

With this drive to multiple distributed constellations, satellites must be smaller, cheaper, and highly efficient. To meet this goal, current satellite subsystems must be miniaturized and packaged efficiently. One of the most important subsystems that must be miniaturized is the propulsion system because of its high percentage of satellite mass and power.

The pulsed plasma thruster (PPT) is an excellent approach for numerous future missions, particularly those that will utilize formation flying within a multiple satellite constellation because of its small impulse bit and high specific impulse. The PPT is a small, self-contained propulsion system that utilizes a solid Teflon® propellant. Teflon has the advantage of being inert and nontoxic, giving the PPT system an additional benefit of being one of the safest propulsion systems for spacecraft.

The PPT, shown schematically in Fig. 1, operates as follows. First, a power-processing unit (PPU) takes power from the satellite bus and charges a capacitor to several thousand volts. Teflon then feeds between a pair of electrodes charged by the capacitor. An igniter, which consists of a semiconductor surrounded by another set of electrodes, fires to allow the capacitor to discharge and ablate a small amount of the Teflon. This Teflon is then accelerated away from the spacecraft as a result of a combination of electromagnetic and gas dynamic forces, producing thrust.

Pulsed plasma thruster technology has a long history of reliable space-flight operation. The first PPT flight was aboard the Soviet Zond-2 spacecraft in 1964 (Ref. 5). In the United States, PPT development work for the present solid-state Teflon devices began in the 1960s and led to a 1966 program with Massachusetts Institute of Technology's (MIT) Lincoln Laboratories to begin development of a Teflon PPT microthruster. This development led to the first U.S. flight of a PPT in 1970 aboard the Lincoln Experimental Satellite (LES 6) spacecraft.[6] This flight unit was a breech-fed design and provided 26 μN of thrust at a specific impulse of 312 s. The system performed flawlessly in an East–West stationkeeping role for the five-year life of the LES-6 satellite.

The success of the LES-6 application lead to consideration of the PPT for other missions. In particular, PPTs were found to be well suited to provide drag compensation for the U.S. Navy's NOVA navigation satellites. Three NOVA spacecraft were launched between 1981 and 1988. Two PPT systems per spacecraft provided drag make-up propulsion for seven years on each of the three NOVA

Received 4 February 2003; revision received 2 January 2004; accepted for publication 8 January 2004.

*Research Assistant, Department of Aeronautics and Astronautics; currently Senior Development Engineer, Systems and Technology Development Department, Aerojet-General Corporation, Redmond, WA 98073. Member AIAA.

†Assistant Professor, Department of Aeronautics and Astronautics; currently Assistant Professor, Sibley School of Mechanical and Aerospace Engineering, Cornell University, Ithaca, NY 14853. Member AIAA.

‡Associate Professor, Department of Aeronautics and Astronautics. Senior Member AIAA.

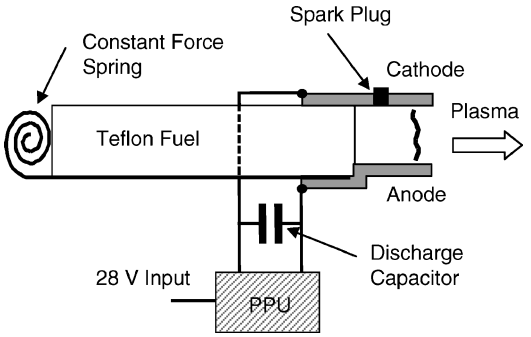

Fig. 1 Schematic of a pulsed plasma thruster.

spacecraft in low earth orbits (LEO).[7] A more complete review of historical thrusters is included in Ref. 8.

In 1995, NASA Lewis Research Center (now Glenn Research Center) initiated a program with Primex Aerospace Co. (now Aerojet-Redmond Operations) to develop, fabricate, and flight qualify a PPT that improved significantly on the then current state of the art. The result is the Earth Observer-1 (EO-1) PPT, which performed flawlessly starting in February of 2001 and is still operational.[9–11]

With the trend in satellite design towards small, low cost, satellite constellations, the need for miniaturizing the PPT (and other thruster systems) is apparent. The objective of this work is to build, test, and validate, in space, an integrated PPT system for the microsatellite (10–100 kg) class, providing formation keeping and maneuvering, orbit maintenance, and attitude control.

A similar effort to miniaturize the pulsed plasma thruster has been undertaken by the U.S. Air Force Research Lab (AFRL) at Edwards Air Force Base. The AFRL Micro-PPT uses a coaxial geometry to provide impulse bits on the order of 10 μN $\cdot$ s (Ref. 12). Initially, two laboratory designs were presented: a self-triggered design and an externally triggered design.[13] Later, a three-electrode design is presented in a desire to reduce shot-to-shot variability in the self-triggered design while allowing for the elimination of the external igniter used in the externally triggered design. Initial life testing at 2.25 J yields an average mass flow rate of 8.6 μg/s while operating at 1 Hz (Ref. 12).

CU Aerospace, teamed with the University of Illinios at Urbana–Champaign and Unison Industries, has also been working toward developing thrusters in the approximately 100-W range. The PPT-10 and PPT-10.1 are side-fed coaxial pulsed plasma thrusters based on the previous PPT-4 (Ref. 14) and PPT-7 (Ref. 15) thruster designs. These thrusters operate at considerably higher energy levels (40–80 J) producing several mN of thrust with a specific impulse of approximately 800 s.

To achieve the desired performance objective within the stringent mass, power, and cost requirements of the micro- and nanosatellite classes, the Dawgstar design is examined at the systems level. This approach contrasts the ongoing research at the AFRL where the design philosophy is to attempt fundamental changes in the PPT topology in order to accomplish significant reductions in the thruster dry mass. Issues such as mechanical size, capacitor selection, and sparkplug design are evaluated, with focus on areas such as lifetime demonstration, system compatibility, and miniaturization of the electronics. This paper describes the mechanical and electrical design, theory, and test results for this thruster, termed a micropulsed plasma thruster (μPPT).

Motivating Mission: Dawgstar and ION-F

The Ionospheric Observation Nanosatellite Formation (ION-F) comprises three 15-kg spacecraft designed and built in cooperation by University of Washington (Dawgstar Satellite), Utah State University (USUSat), and Virginia Polytechnic Institute and State University (HokieSat) in order to develop a space-based distributed control and science testbed. The ION-F mission objectives are formation flying, including in-track and ground-track maneuvering and station keeping[16]; simultaneous, spacially distributed measurements of the ionospheric electron density[17]; and PPT-enabled attitude and orbit control. A novel feature of the mission is the planned suite of formation-flying control experiments involving the three satellites. The ION-F mission is part of the AFRL Air Force Office of Scientific Research (AFOSR)/DARPA/NASA University Nanosatellite Program, which provides technology development and demonstrations for future Air Force and NASA distributed satellite systems, such as TechSat21.[18] The ION-F satellites are being designed and built by students at the three universities, with close coordination to ensure compatibility for launch, deployment, and the formation-flying mission. The three universities are coordinating in the areas of satellite design, formation flying, mission development, and scientific instrumentation. The ION-F satellites contain all of the capabilities necessary to demonstrate multiple spacecraft distributed control, including propulsion, intersatellite communication, and global-positioning-system (GPS) measurements.

Table 1 Summary of Dawgstar propulsion requirements

Requirement	Value
Peak power consumption	13 W
Power supply voltage	28 V
Mass	4.4 kg
Interface temperature range	−40–60°C
Total ΔV[a]	75 m/s
Burn time[b]	<75 days
Lifetime	≥1.5 million pulses
Warm-up time	<1 s
Maximum firing rate (per thruster)	2 Hz

[a]Based on 15-kg satellite.
[b]Defined as the total time to deliver the required ΔV.

The Dawgstar propulsion system is required to fulfill the three major requirements of the propulsion system: attitude disturbance rejection, distributed formation flying, and limited orbit maneuvering. Performance requirements, shown in Table 1, are generated based on available power and mission objectives.

Formation Flying and Propulsion Requirements

The ION-F mission will demonstrate formation flying using its unique control capability. Formation flying is defined as two or more spacecraft using an active control scheme to maintain the relative positions between the spacecraft.

Autonomous formation flying using intersatellite cross-links has yet to be demonstrated. There are many cases of rendezvous in the past, and EO-1 has flown in formation with Landsat.[11] However, the latter case was accomplished using satellite-ground communication links, rather than autonomously using satellite cross-links. The ION-F formation-flying mission objectives are to 1) demonstrate intersatellite communications, 2) demonstrate autonomous formation keeping, and 3) demonstrate autonomous formation maneuvering. If time permits, more than one formation, three satellite maneuvers, and coordinated attitude control will also be demonstrated.

The ION-F formation flying mission will primarily focus on the leader–follower formation. The leader–follower formation is exactly as the name implies: identical orbital parameters but at different times. Once the three satellites deploy and check out, each of the satellites drift apart because of the separation velocity and differences in drag; the separation is largest in the radial path. The ION-F satellites then perform a series of experiments using the formation's control capability, evaluating control architectures and algorithms.[19,20] Additional formations, such as the same ground track formation and local cluster ellipses, will be flown if time permits.

Based on an initial study of the power generation, formation control capability, and lifetime for Dawgstar and ION-F, Table 1 shows a summary of the requirements placed on the propulsion system design.

A trade study was conducted for the Dawgstar propulsion system, comparing the two most viable propulsion system candidates based on the defined requirements: pulsed plasma thrusters and cold gas thrusters.[21] The PPT design was assumed to be a scaled version of

the larger EO-1 system developed at Primex Aerospace Co. (now Aerojet-Redmond Operations). The baseline energy of 5 J was derived from power requirements, and a specific impulse of 500 s was assumed based on worst-case scaling from the EO-1 PPT. A full comparison and discussion of the differences between the miniaturized PPT and a cold gas thruster is given in Ref. 21. Although both systems are capable of compensating for the expected disturbance environments, the PPT was selected because of its lower overall mass and higher reliability as a result of no concerns about propellant leakage. In addition, PPTs in general require no warm-up time, offer discrete impulse bits, are failsafe, and have an extended shelf life.

Proposed Hardware Architecture

For Dawgstar, the proposed propulsion system consists of eight thrusters providing direct control in two axes for translation and three axes for rotation. The sixth axis (elevation) can be controlled via orbital dynamics. Placement of thrusters maximizes the mobility of Dawgstar. The final configuration has eight thrusters mounted in four orthogonal pairs at the top and bottom of the satellite, as seen in Fig. 2 and Table 2. Each of the four thruster modules consists of two thrusters mounted orthogonally, with two fuel bars at a 45-deg feed angle, which allows orthogonal thrust and saves volume. One discharge capacitor is used for each module for a total of four discharge capacitors in the propulsion system. The system is designed such that two thrusters from separate modules (two of the four) are fired when thrust is required. As an example, firing thrusters 6 and 7 produces thrust in the x direction, firing thrusters 2 and 6 produces rotation about the z axis, and firing thrusters 3 and 6 produces rotation about the y axis. Thruster placement and firing combinations are illustrated in Fig. 2 and Table 2.

Table 2 Dawgstar thruster firing combinations

Motion	x axis	y axis	z axis
Translation	(2, 3)	(4, 5)	——
	(6, 7)	(1, 8)	——
Rotation	(1, 4)	(2, 7)	(1, 5) (2, 6)
	(5, 8)	(3, 6)	(3, 7) (4, 8)

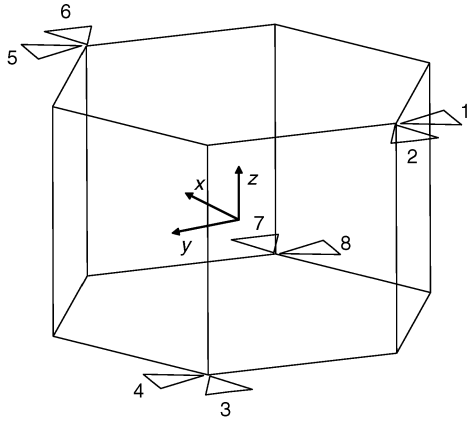

Fig. 2 Dawgstar thruster placement.

Because of the limited resources on Dawgstar, both the power and mass must be reduced considerably from previous designs such as EO-1. One obvious area of change to achieve power reduction is the PPU. Current designs for two thruster systems consist of a charge converter for one capacitor and two discharge circuits.[9] For Dawgstar, each thruster module (consisting of two thrusters) uses this configuration; however, one power-processing unit and high-voltage electronic switching circuits are used to charge the correct thruster modules.

Flight Design

Mechanical

The design of the flight thruster assembly is based primarily on maximizing the thrust-to-power ratio within the mass and volume constraints placed by the Dawgstar program. Because the thrusters are placed in pairs, it is desirable to package them together in the mechanical design. This integrated packaging is the key design feature for minimizing the mass of the mechanical system. In this design, the full thruster assembly is placed on top of the single capacitor, then attached directly to the top and bottom structural panels of the satellite. The thruster assembly is machined from Ultem 2300, a glass-filled thermoplastic. Ultem is used because it has one of the highest strength-to-weight ratios of materials that met the temperature and dielectric strength requirements. The thruster is manufactured in two parts to facilitate ease of machining. Two Teflon fuel bars are fed in parallel into each of the thrusters comprising the PPT module using constant force springs. The face of each fuel bar is cut at a 45-deg angle. The fuel bars lie as mirror images to each other, which allows the thrust vectors of the pair to be perpendicular as they leave the module. The tip of each fuel bar is then in contact with the anode, which acts as a stop. The flight design for the Dawgstar PPT is shown in Figs. 3 and 4.

A detailed view of the electrodes and strip lines with the thruster housing removed is shown in Fig. 4. Both the top and bottom strip lines are at cathode potential allowing two current paths to the active cathode. A third, anode strip line connects the bottom of the anode to the capacitor and is not shown in Fig. 4. The boron-nitride insulators serve to contain the plasma when it is first created. A small lip at the back of these insulators prevents excess charring of the top and bottom of the Teflon fuel bar, which can cause the cathode and anode to short during operation. Between the two boron-nitride insulators is a labyrinth, which prevents shorting along the surface of the boron nitride as a result of carbon deposition.

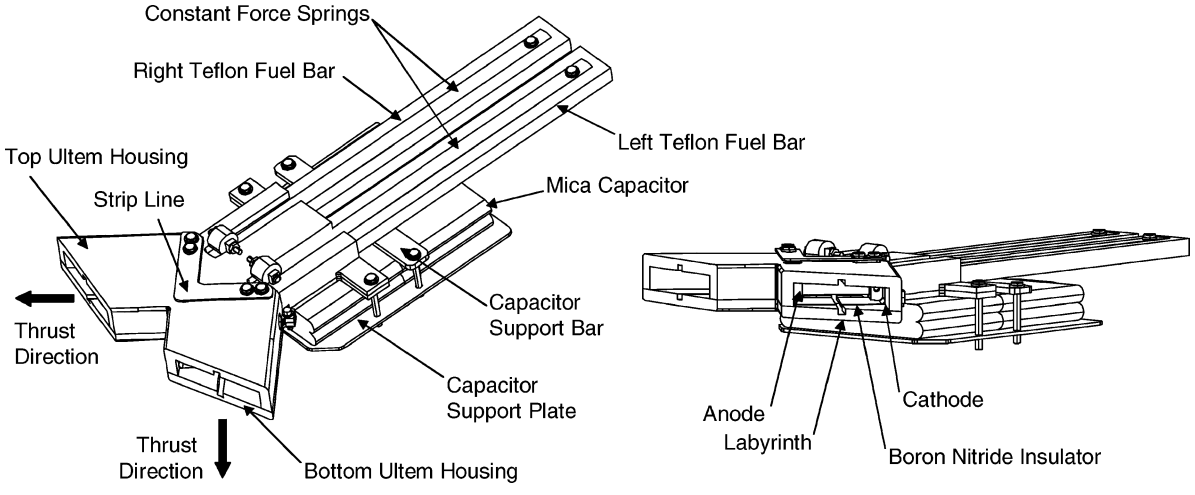

Fig. 3 Dawgstar pulsed plasma thruster.

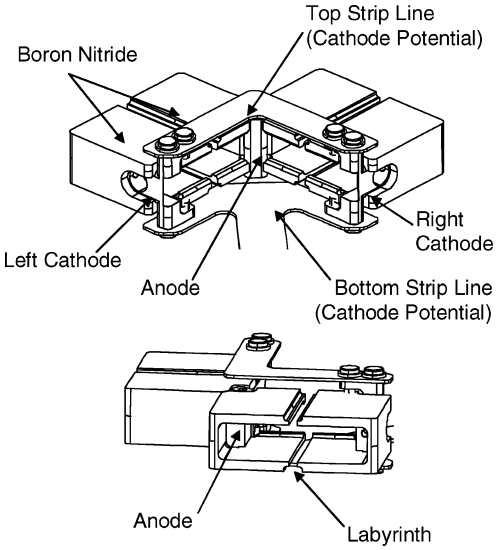

Fig. 4 Electrode and strip-line detail.

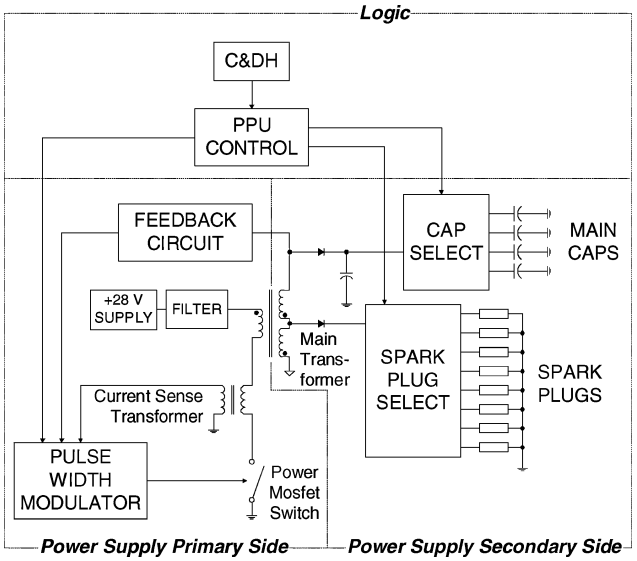

Fig. 5 Dawgstar power-processing unit functional block diagram.

Each cathode is constructed using oxygen-free, high-conductivity copper. Flanges at the top and bottom are used to connect the cathode to the strip lines. An igniter, which triggers the discharge of the thruster, is mounted in the center of each cathode. As a final step to ensure that the anode and cathode do not short, a small gap is introduced between the edge of the fuel bar and the cathode. The thruster is designed such that if carbon is deposited on the face or front edges of the fuel bar (where it is not protected by the boron nitride) shorting will not occur. Electrode erosion is generally much more severe at the anode than at the cathode; the anode for both thrusters is machined from a single piece of stainless steel to mitigate this effect. The strip lines are designed such that their thickness is much greater than the skin depth for a copper-carrying current with a frequency of 500 kHz. The routing of the strip lines is designed to minimize external inductance by keeping both strip lines as close to each other as possible. In this case, the Ultem housing passes between the strip lines and the boron nitride. The strip lines are wrapped in Kapton tape to prevent arcing to the adjacent structure or other parts internal to the satellite.

After initial testing was conducted on the engineering unit, a modification was made in the strip line design. The copper strip lines were initially bolted to the strip line in the center of the part. The cathode was then split to carry current both above and below the Teflon bar to the electrode. Near the anode, the cathode was shielded with a 1.3-mm-thick Ultem barrier designed to insulate the cathode electrically and prevent arcing between the anode and cathode strip lines. This assembly was then placed inside the top and bottom Ultem housing. During testing, the strip lines initially performed as anticipated, but after several thousand firings of the thruster carbon from the decomposition of the Teflon began to deposit on the sides of the Ultem insulator. Eventually, deposited carbon provides a path for arcing to occur. In the final design the cathode strip lines are moved to the outside of the Ultem parts such that there are no breaks or edges in the barrier between the anode and cathode. This change greatly decreased the potential for arcing between the strip lines and the anode.

Electrical

The requirements of the PPU are to charge two of the four 1.3-μF main capacitors to 2.8 kV at a rate of 1 Hz with an option to charge twice as fast. Additionally, the PPU must generate a pulse of greater than 1.5 kV to two of eight igniters to initiate discharges on selected thruster. The discharge-initiation (DI) circuit must deliver approximately 0.3 J to the plugs, at peak currents of $\sim$200 A. Input power to the PPU is nominally 28 V with a range of 24–32 V. The PPU utilizes a flyback switch-mode power supply (SMPS) converter operating in discontinuous mode to provide the charging voltages: 2.8 kV for the main capacitors and 1 kV for the 0.68-μF DI capacitors, generated on secondaries of the flyback transformer. A resonant tank circuit is used by DI circuitry to double the voltage of the DI capacitor for discharge initiation.

The PPU is composed of three functional units: the primary side, secondary side, and logic, as shown in Fig. 5. The primary side delivers current pulses to the flyback transformer primary. The secondary side distributes the energy stored in the transformer to selected main and DI capacitors via high-voltage switches. In the flyback topology, the transformer is connected such that the secondary windings are of opposite polarity from the primary windings. During current injection into the primary, current is prevented from flowing in the secondary by rectifier diodes. The primary windings then act as a simple inductor until the switch opens. When the desired energy has built up in the primary, the switch is opened, causing the voltage to reverse polarity (or fly back). The opening of the switch-forward biases the rectifiers on the secondary, and energy stored in the transformer is delivered to the capacitors. The logic unit controls the charge rate and high voltage switches.

The primary side utilizes a pulse-width modulator (PWM) to turn current on and off in the transformer primary via a MOSFET switch. The output signal from a current-sense transformer is fed to the PWM, which then is able to interrupt current flow at a specified primary current for each pulse. The pulse frequency, set by a resistive-capacitive (RC) network on the PWM, is chosen to be 20 kHz based on extensive experimentation to optimize efficiency. To charge at twice the nominal rate, the frequency is increased to 44 kHz using a logic signal that changes the resistance in the RC network. Because the converter operates in discontinuous mode, each pulse delivers nearly the same energy to the primary, so that the input power to the converter is constant during charging. The capacitor energy increases linearly in time, and the voltage is proportional to the square root of time.

After trials of several SMPS transformer designs, an E-core was selected on the basis of efficiency and relative ease in insulating windings against arc-over. The primary has 21 turns of 22 American Wire Gauge (AWG) high-temperature, 5-kV rated magnet wire, and the core is gapped to yield a primary inductance of $\sim$100 μH. The load resistor on the current-sense transformer is selected such that the peak primary current is 3.6 A, which yields an input power of approximately 13 W at 20 kHz. The secondary has two sets of windings, one with 166 turns to provide the DI charging voltage and a second with 284 turns, each using 32 AWG, 3.5-kV rated magnet wire. The main capacitors are charged by both secondary windings in series (450 turns). Winding layers are separated by high-voltage tape, and the transformer is vacuum impregnated with varnish.

A 1000:1 voltage divider on the discharge capacitor supply is fed to a comparator with a 2.8-V reference voltage in order to terminate charging and initiate discharge when the capacitor voltage reaches 2.8 kV. At the onset of charging, a one-shot multivibrator

with a period of 2 s is initiated. In the event of a malfunction that prevents the capacitors from reaching 2.8 kV during charging, the multivibrator output will initiate a discharge.

The secondary side of the PPU distributes the energy generated by the primary side to the proper main capacitors and discharge initiation circuits. Opto-isolators with zero-crossing triac outputs rated at 800 V are used to switch the secondary voltage to the selected capacitors. Each switch for 2.8 kV uses five opto-isolators in series (4-kV total rating), and each DI switch uses two optoisolators in series (1.6-kV total rating). Resistors (22 MΩ each) are placed across each opto-isolator output to distribute voltage evenly. The secondary-side switching topology is illustrated in Fig. 6. The use of high-voltage output switching enables a considerable reduction in the electrical system mass when compared to previous designs that utilized multiple high-voltage generation circuitry.

To avoid the large mass associated with using high-current step-up transformers to provide the $\geq$1.5 kV needed to initiate discharges on the DI ignitors, a resonant tank circuit design was used. Illustrated in Fig. 7, the circuit uses a 1.2-kV insulated gate bipolar transistor (IGBT) to switch the 1-kV voltage on the DI capacitor to a tank circuit composed of a 15-μH high-current inductor and 10 nF, 3-kV ceramic capacitor. The 10-nF capacitance is much larger than the capacitance of the DI feed cable and plug, yet much less than the 0.68-μF DI energy storage capacitor. In principle, the peak ringing voltage is twice the DI capacitor voltage, or approximately 2 kV, because the damping is small prior to discharge. A Y5V temperature coefficient is chosen for the ringing capacitor because it has a relatively large voltage coefficient. This results in a peak ringing voltage of approximately 2.5 kV, leading to a very reliable spark

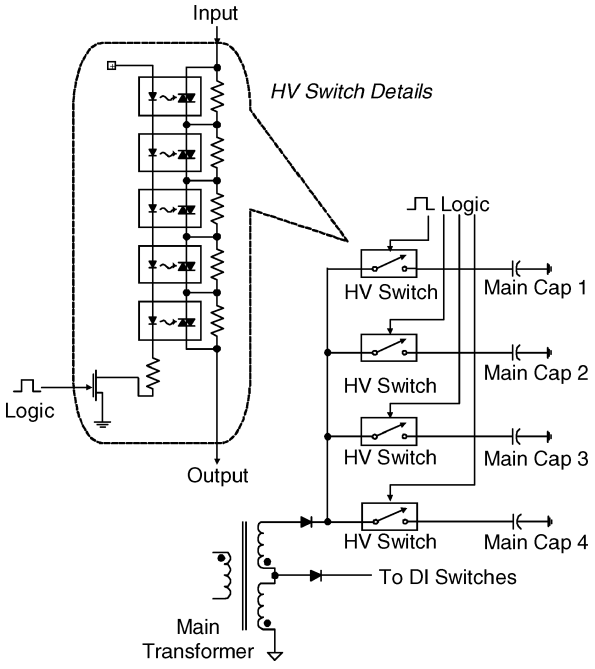

Fig. 6 High-voltage switching for the main capacitor.

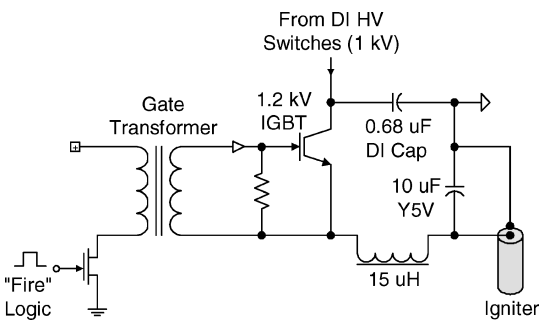

Fig. 7 Discharge initiation pulse circuit using ringing tank.

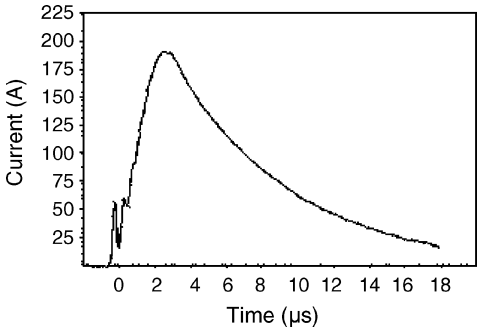

Fig. 8 Discharge initiation current profile.

initiation. Over 30 different commercial off-the-shelf (COTS) inductors were tested before selecting the 15-μH, iron-core flight unit. Key considerations included low saturation, fast rise time, and high density. Ferrite-core inductors were found to saturate easily, leading to runaway currents and failure of the IGBT. Although the flight unit (Fastron model MESC-150M-01) is rated for 2 A dc, very little saturation is observed for discharge pulses at currents up to 300 A (discharge duration $\sim$2 μs). A typical discharge initiation circuit current profile is shown in Fig. 8.

Satellite Communication Interface

The flight computer sends serial signals [Data (D), Clock (Ck), and Fire (F)] to control the main capacitor and DI selection and charging. Data on the D line are clocked into a HC174 serial-to-parallel logic IC by the clock line (eight clock pulses) and have high bits for each of the DI circuits to be selected. All inputs to the PPU control circuit are isolated using opto-isolators. The high-to-low transition of F initiates charging of the appropriate capacitors. (The proper DI selection lines having already been set.) During capacitor charging and firing, a "busy" output signal is held high. The flight computer uses this digital signal to determine when the PPU fires before reinitiating another charge cycle.

If the desired charge time for the system is less than 1 s, a fast charge mode can be enabled. This is accomplished by holding the D signal high when the transition of F occurs (after the selection of the appropriate DI).

Theory and Testing for Component Design

Theory

The derivation of analytical formulas that accurately predict the behavior of PPTs has proven difficult historically. Following Guman,[22] it is possible to derive several simplified equations that describe the characteristic features of the thruster by considering thrust to be a combination of magnetic and gasdynamic forces.

Considering the magnetic contribution first, the magnitude of the impulse can be determined by finding the instantaneous magnetic pressure on the back wall and integrating this with respect to time over the length of the pulse. In the idealized case, the magnetic field is assumed to be generated by a uniform current sheet. The resulting instantaneous force is calculated as the magnetic pressure times the area:

$$F_{\text{instant}} = B^2/2\mu \cdot A \tag{1}$$

Under the assumption of a uniform current sheet, the magnetic field strength is proportional to the current i divided by the separation, and the area is simply the width of the electrodes times the separation, yielding

$$F_{\text{instant}} = \mu/2 \cdot A_R \cdot i^2 \tag{2}$$

Integrating the instantaneous force over the time of discharge, the force produced as a result of magnetic pressure alone is

$$T_{\text{magnetic}} = \frac{1}{2} f \mu A_R \int_0^t i^2 \cdot \mathrm{d}t \tag{3}$$

Current is either estimated through the analysis of an underdamped resistive-inductive-capacitive (RLC) circuit or determined

experimentally. Experimentally, we know that the current undergoes damped oscillation with an initial voltage V_0, leading to the relation

$$i = V_0/L\lambda \cdot e^{st} \cdot \sin(\lambda t) \tag{4}$$

where

$$\lambda = (1/LC - R^2/4L^2)^{\frac{1}{2}}, \qquad s = R/2L$$

Further, assuming uniform current the nozzle inductance is approximated as

$$L = \mu \cdot A_R \cdot l \tag{5}$$

Also noting

$$P = f\left(\tfrac{1}{2}CV_0^2\right) \tag{6}$$

substituting Eqs. (4–6) into Eq. (3), and taking the limit as $t \to \infty$ yields

$$T/P|_{t\to\infty} \to \mu A_R/2R \tag{7}$$

Experience indicates that PPTs also produce a thrust contribution from gasdynamic expansion. Again following Guman,[22] a volume element that isentropically expands into a vacuum after the addition of energy E is considered. If the element is sufficiently thin such that nonsteady pressure waves rapidly transverse the element, the mass-averaged flow velocity is equal to the sonic velocity, and the initial temperature is large compared to the final temperature. For this case, the thrust as a result of gasdynamic expansion can be written as

$$T_{\text{GAS}} = f\{[8(\gamma-1)/\gamma^2(\gamma+1)]m_D E\}^{\frac{1}{2}} \tag{8}$$

Based on Eqs. (7) and (8), the total thrust-to-power ratio is shown to be proportional to several important parameters:

$$T/P \propto A_R \Big/ R\sqrt{E/m_D} \tag{9}$$

This equation forms the basis for the optimization of the Dawgstar PPT.

Aspect-Ratio Optimization

Equation (9) shows that in order to maximize the specific power one option is to maximize the aspect ratio. Yuan-Zhu[23] shows that for a 4.26 J breech-fed PPT with a propellant area of 2.0 cm^2 increasing the aspect ratio from 2.0 to 3.13 translates to a 57% increase in impulse bit and a 26% increase in specific impulse with no increase the power consumption. Further improvements of this magnitude can also be achieved at several different aspect ratios, areas, and energy levels. Work by Palumbo and Guman[24] shows that for side-fed PPTs the spacing between electrodes must be tuned in order to optimize the performance; specifically the work shows that as the electrode spacing increases beyond an optimal point, efficiency begins to decrease.

For the Dawgstar PPT design, it is clear from the Yuan-Zhu results that the aspect ratio should be high. Because extensive study of aspect-ratio variations is not within the scope of this project, the aspect ratio is chosen to be 4.0, which is within the range for which Yuan-Zhu presented data.

Strip-Line Design

The initial strip-line design provided insufficient isolation between the anode and cathode strip lines resulting in arcing. To mitigate this, an alternative strip-line design was adopted, which located the strip lines on the outside of the Ultem housing and removed a center post that was at cathode potential. Conceptually, changing the strip lines in this way will result in 1) an uneven current distribution between the top and bottom cathode strip lines, 2) a change in magnetic field strength and direction in the region containing the plasma, and 3) an increase in the total circuit inductance. Testing and theoretical calculations were completed in order to quantify the magnitude of these effects.

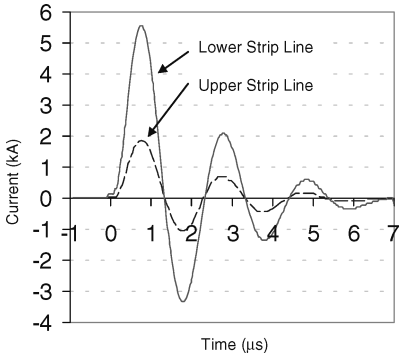

Fig. 9 Typical discharge current traces for the Dawgstar PPT.

For puposes of strip-line evaluation, Rogowski coils are installed around all strip lines in the thruster module. The Rogowski coils were custom designed to meet size constraints and were subsequently calibrated to a Pearson probe with a known response.

The current results for a single pulse as measured by Rogowski coils on the top and bottom cathode strip lines are shown in Fig. 9. The results indicate that 66% of the current flows directly from the capacitor to the active cathode along the shortest route. The additional current travels through the cathode on the nonactive side of the assembly and the top strip line to reach the active cathode. The ringing in this current profile is more severe than the actual implementation because of changes in strip-line layout, which were made to accommodate a Pearson probe used for calibration.

Because of varying strip-line separation distances and differential current distributions, the actual magnetic field created differs from both the optimum design conditions and the initial design. To estimate the relative differences between each of these conditions, the magnetic field created by two current-carrying wires (modeling strip lines) is calculated using MATLAB®. In all cases, the only parameters varied are the wire separation distance and the proportion of the total current carried in each wire.

Figure 10 shows a cutaway view of the thruster looking toward the cathode with the Ultem housing removed for simplicity. In the plots, the solid contour lines represent lines of equal magnetic field strength while the arrows depict the magnitude and direction of the negative gradient of the magnetic field. These arrows are then representative of the magnitude and direction of magnetic force on the plasma from the strip lines.

Based on the results of Fig. 10, the difference in magnetic field strength from the strip lines does not appear to cause a significant change in thrust magnitude or direction. Although the direction of the magnetic field is initially skewed off axis at the rear of the channel in the final configuration, the magnetic field throughout most of the acceleration region is not significantly different in magnitude or direction.

A measurement of the change in actual circuit inductance was not within the scope of work completed. A simplified analysis based on increase in area between the strip lines, measured currents, and calculated magnetic fields shows that the increase in induction of the strip lines should be on the order of 4 nH. This increase in induction is small when compared to a total measured inductance of approximately 67 nH. Based on the thrust-to-power equation presented, this change in inductance should result in a decrease in thrust of less than 6% at constant power.

Capacitor Testing

The PPT requires very short-duration, high-amplitude current pulses to achieve its characteristic electromagnetic and concentrated gas-dynamic acceleration. Previous thrusters have almost exclusively utilized oil-filled capacitors for this purpose. Various capacitor technologies were tested in a concurrent effort undertaken by Aerojet, the NASA Glenn Research Center, and Unison Industries in association with the Dawgstar PPT program. Capacitor types tested included the baseline 40-μF Maxwell oil-filled capacitor (LES 8/9 and EO-1 heritage), a COTS 39-μF AVX Corp. stacked ceramic

Table 3 Summary of the experimental characteristics of the Dawgstar flight unit

Parameter	Fast charge mode	Slow charge mode
Impulse bit I_{bit}	66 ± 4 μN · s	60 ± 4 μN · s
Specific impulse I_{sp}	266 ± 40 s	242 ± 40 s
Typical firing time	440 ± 5 ms	940 ± 5 ms
Peak PPU input power	36.0 ± 0.4 W	15.6 ± 0.3 W
System thrust-to-power ratio	9.7 ± 0.6 μN/W	9.0 ± 0.6 μN/W
Thruster thrust-to-power ratio	13.3 ± 1.0 μN/W	12.3 ± 1.0 μN/W
Thrust range	60 ± 4 μN to 264 ± 18 μN	
Mass loss per firing m_D	25.3 ± 0.8 μg	
Discharge capacitor energy per firing E	4.9 ± 0.2 J	
Ignition circuit energy per firing	0.3 ± 0.1 J	
Lifetime	>1.7 million pulses	
Thruster efficiency	$1.8 \pm 0.5\%$	
PPU converter efficiency	$78.0 \pm 4.0\%$	
PPU standby current	$<10 \pm 1$ mA	

[a]Excludes electronics and igniter.

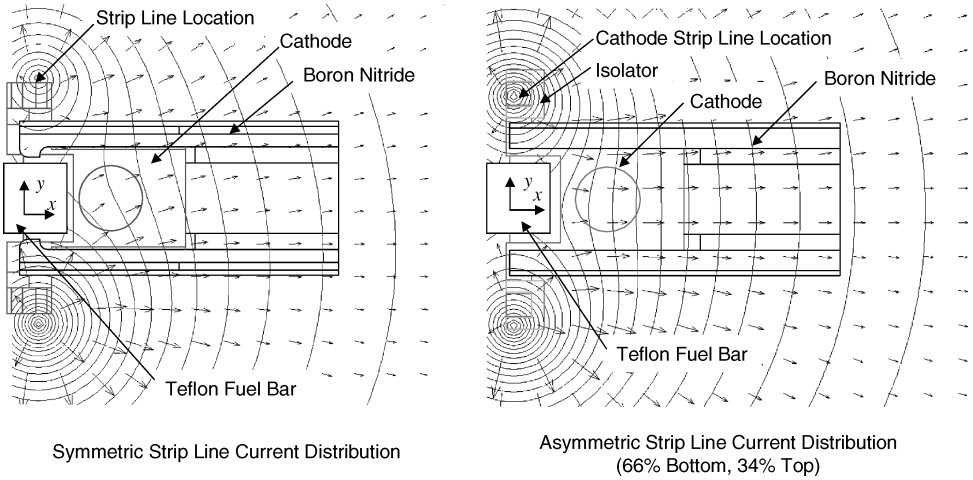

Fig. 10 Magnetic field lines plotted with the thruster hardware.

capacitor, a 5-μF Unison Industries mica-paper/foil capacitor, and a 45-μF metallized film capacitor provided by Auburn University. Tests were designed to evaluate the behavior of different types of capacitors with the same thruster load and included a consistent energy level so that direct comparison is possible.

All four capacitors tested provided sufficient discharge current for the PPT. Of the four capacitors tested, three survived the 10,000–30,000-pulse duration of the tests, with the stacked ceramic capacitor failing after 4450 pulses. In this case, a fracture of the ceramic at the lead was found to be the failure point, most likely as a result of piezoelectric effects. Of the remaining capacitors, the mica-paper/foil capacitor had a combination of acceptable energy density, dry impregnant, flat geometry, and easy scaling to a smaller size, leading its selection as the capacitor technology for the Dawgstar PPT.

Sparkplug Testing

Discharge igniter testing was conducted at the University of Washington in conjunction with Aerojet and Unison Industries. The purpose of these tests was to characterize a new, smaller 6.35-mm-diam igniter developed by Unison, evaluate different igniter materials, verify the 45-deg propellant feed angle over several million pulses, obtain a second measure of Teflon flow rates, and perform capacitor lifetime testing on the mica-paper/foil capacitor.

Three igniters with different materials were successfully tested to 1 million pulses each, while the breakdown voltage and igniter resistance was measured. Misfire rates for all three igniters were less than 2% after an initial period of conditioning that can last as long as 100,000 pulses. The minimum igniter voltage required to trigger a complete discharge was measured periodically. The results show ignition voltages in the several hundred voltage range after the conditioning period.

Another significant result of these tests was the validation of the Teflon feed system with its 45-deg feed angle. Approximately 10 cm of propellant was fed for each of the 1 million pulse tests without any indication of cold flow or significant uneven ablation.

System Ground Testing

Ground testing was completed using two thruster units: a flight prototype unit and a flight spare. Endurance, mass loss, and electrical testing was conducted on the flight prototype unit while thermal, vibration, performance, and electromagnetic interference (EMI) testing were completed on the flight spare. Integrated acceptance testing was performed on each of the flight units and electronics prior to integration with the satellite. The flight prototype unit and the flight units were identical except for the mounting interface and capacitor. The capacitance (2.7 μF) and construction (mica-paper and foil) of the flight and flight spare capacitors is the same, while the manufacturer and mechanical interface differ. The resulting performance for the Dawgstar PPT is summarized in Table 3. Uncertainty values are reported with 95% confidence.

Performance

Thrust measurements on a flight prototype thruster were conducted at the NASA Glenn Research Center on a torsional thrust stand.[25,26] Prior to taking thrust measurements, the system was operated for approximately 10 min to allow the thruster and electronics to come to thermal equilibrium. When operating the PPU in slow charge mode, samples were collected for 1 min with the thruster firing at 1 and 2 Hz. Displacement was measured corresponding to thrust levels of 119 ± 3 μN and 61 ± 4 μN with an average impulse bit of 60 ± 4 μN · s. Data were also collected during 2-min runs for firing rates of 1, 2, and 3 Hz while operating in fast charge mode.

Thrust was calculated as 199 ± 3 μN, 133 ± 3 μN, and 64 ± 4 μN with an average impulse bit of 66 ± 4 μN · s. Input voltage and current measurements taken at the chamber wall show a total input energy to the PPU of 7.2 ± 0.1 J during fast charge and 6.4 ± 0.1 J during a slow charge. No correction was made for the expected voltage drop in the cables between the chamber wall. The total firing time, defined from the time the PPU first draws power until thruster firing, was also measured at 236 ± 5 ms (fast charge) and 430 ± 5 ms (slow charge). The maximum theoretical thrust of 264 ± 18 μN was not demonstrated experimentally.

Electrical

Extensive testing of the performance and reliability of the PPU design was conducted during the development phase with a series of prototype units. Because the PPU behavior was verified via this testing, ground testing of the flight unit was primarily used to verify basic electrical functionality. Ultimately, the reliability shown in the lifetime tests ("Lifetime" section) validates the performance of the PPU electronics.

The first tests verified that the proper capacitor(s) are selected based on logic input signals. For these tests, although the DI ignitors are fired normally, they were not placed in proximity to the PPT electrodes, because of the deleterious effects of firing the PPTs in air. The main capacitors are resistively discharged. The tests validated correct selection of main and DI capacitors for all possible switch selections. Although designed originally to charge two capacitors per shot, the PPU can select 1, 2, 3, or all 4 capacitors for charging by selecting appropriate control input signals. All combinations were successfully tested.

The next test verified proper charging voltages. The main capacitor charge voltage was measured to be 2.74 kV at the time of discharge initiation, and the DI capacitor voltage was measured to be 1.00 kV. These charge voltages did not vary with bus input voltage or number of capacitors charged.

Charge times were measured over the full range of bus voltages, for slow and fast charge, and for various numbers of main capacitors selected. When operating in slow charge mode, charge times were 470 ± 2 ms/capacitor (charging one to four capacitors) and when operating in fast charge times were 220 ± 1 ms/capacitor (charging one or two capacitors).

A current integrator was used to determine the total input charge to the PPU during each cycle. For the slow charge rate of two capacitors at a 28-V bus voltage, the measured input energy was 13.4 J. The calculated energy delivered to main and DI capacitors was 10.43 J, resulting in a PPU efficiency of 78%. The PPU design was optimized for low power consumption, and when not charging the current consumption is <10 mA.

Table 4 Random vibration test parameters

Frequency, Hz	Power spectral density, g^2/Hz
20	0.025
20–50	+6.0 dB/oct
50	0.15
600	0.15
600–2000	−4.5 dB/oct
2000	0.025

Lifetime

Endurance testing was completed at the University of Washington with the flight prototype thruster. During a first set of tests, the PPT accumulated in excess of 1.1 million pulses over 153 h of continuous firing at 2 Hz, which mimics the most strenuous expected conditions. Subsequent testing completed to collect thermal and mass loss data resulted in an additional 0.6 million pulses, bringing the total number of pulses to 1.7 million. During all tests, the thruster and prototype electronics performed flawlessly.

Thermal

Thermal testing was undertaken to estimate the heat load generated by the pulsed plasma thruster and to verify performance at expected on-orbit conditions. The test was conducted with the qualification unit mounted to the bottom panel of the satellite utilizing the flight interface. The bottom panel was then mounted to a large thermal mass used to simulate components of the thruster that were not present during the test. The thruster, bottom panel, and thermal mass were then thermally isolated from the vacuum chamber using standoffs and insulating blankets.

In the first stage, a 6.3-W heater was used to heat the entire assembly to 40°C. To estimate the amount of heat loss in the system, the heater was turned off, the temperature decay monitored, and the experimental specific heat of the system determined. The flight spare thruster was then fired at 2 Hz, and the resulting temperature as a function of time was recorded. These data show that during steady-state operation 2.2 ± 0.2 J is transferred to the structure each time that the thruster fires. This testing also demonstrated that the thruster operates normally at interface temperatures of 40°C.

Shock and Vibration

Acceptance level sine burst and random vibration tests were completed at Aerojet-Redmond Operations with a single thruster module mounted to the satellite structure. Sine burst testing was used to apply a quasi-static load to the thruster as a simulated strength test. Testing was completed at frequencies between 38 and 40 Hz (approximately one-third of the satellite fundamental frequency) and at a magnitude of 38 g. Random vibration testing was completed in the satellite x, y, and z axis at a magnitude of 12.9 g (rms) for one minute. The vibration test parameters are included in Table 4. No damage to the propulsion system was observed during vibration testing.

Electromagnetic Compatibility

Coupling of radiated EMI emission from the Dawgstar PPT to flight model GPS patch and cross-link monopole antennas was measured. The thruster and antennas were arranged on a spacecraft mock-up to simulate the actual flight configuration and then mounted in a radio-frequency (RF) transparent glass bell-jar vacuum facility (VF55) at the NASA Glenn Research Center. A standard EMI test antenna (log periodic dipole) was located external to VF55 at 1 m from the PPT source to measure EMI emissions at the designated frequencies using conventional methods. Table 5 summarizes the results of this testing.

Table 5 Radiated EMI test results

Parameter	Measurement technique	S-band antenna results	GPS antenna results
Center frequency	N/A	2.060 GHz	1.57542 GHz
In-band measurement (1-MHz bandwidth)	Spectrum analyzer (fixed-tuned mode)	−51 dBm	−31 dBm
In-band measurement (275-MHz bandwidth)	Spectrum analyzer (band-swept mode)	N/A	−1 dBm
In-band measurement (285-MHz bandwidth)	Spectrum analyzer (band-swept mode)	−26 dBm	N/A
Out-of-band measurement (10 MHz to 18 GHz)	Diode detector and digital scope	−8 dBm	+12 dBm
Radiated EMI at 1 m	Spectrum analyzer and EMI Antenna at center frequency	81 dBμV/m/MHz	80 dBμV/m/MHz

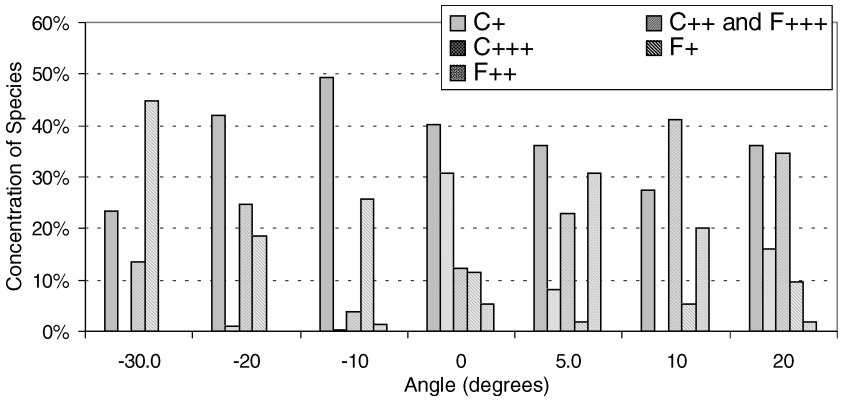

Fig. 11 Dawgstar ion species composition within the plume at various angles.

To measure the in-band component of EMI signal, a preselected spectrum analyzer was employed as a receiver in both fixed-tuned and band-swept mode at 1-MHz resolution bandwidth. Total out-of-band EMI was measured by independently connecting the antenna cables to a 50-Ω input impedance coaxial diode detector that had a calibrated response from 10 MHz to 18 GHz. The diode detector output was connected directly to a 2-GS/s digital storage oscilloscope. Large shot-to-shot variation was observed in the amplitude of the detected EMI events. The adopted procedure reports the largest event of the approximately 100 firings captured during each sample. Additional details of this and other EMI testing involving PPTs are included in Ref. 27.

To reduce conducted EMI from the converter to the satellite bus, a 39-μF ceramic SMPS capacitor is used at the flyback transformer input, along with a common-mode filter and two Pi filters between this capacitor and input bus. Testing revealed that the voltage fluctuations on the bus during charging were $\sim\pm 0.2$ V, measured at 20-MHz bandwidth. Auxiliary voltages ($+5$V, $+12$V) required by the PPU are generated within the unit in order to prevent EMI generation on the satellite auxiliary voltage lines. As just noted, all logic signals to/from the PPU are opto-isolated, so that little EMI is conducted to these signal lines from the PPU.

Plume Characterization

Testing undertaken by others at the University of Washington evaluated plume composition and energy distributions. To determine the relative concentrations of the plume components, a gridded energy analyzer combined with a time-of-flight measurement is used. The analysis assumes a Maxwellian distribution with a characteristic mass-to-charge ratio and drift velocity. A least-squares fitting program using the mass-to-charge ratio and plasma temperature written in MATLAB is used to fit the Maxwellian distribution function to the data. This method gives a least-squares solution for plasma temperature at 2.3 eV, which is consistent with previously measured plume temperatures of 1.8 to 2.6 eV found by others.[28,29]

Figure 11 shows the ion species composition within the plume at different angles. Angles toward the anode are defined as negative and those toward the cathode as positive. Zero is defined as perpendicular to the face of the fuel bar. C^{++} and F^{+++} are combined because the similarity of there mass-to-charge ratios does not allow for differentiation. The concentration of molecular ions (CF^+, C_2^+, F_2^+) is below 10% for all angles tested with the exception of C_2^+ at -5 deg, where the concentration was approximately 13%. The results show that the plume is not symmetric and the composition of ions cannot be assumed to be the same throughout the plume. Additional details are included in Ref. 30.

Mass Properties

The total propulsion system measured mass is 4.20 kg and includes eight thrusters (four modules), propellant, all associated electronics, capacitors, hardware, cabling, temperature sensors, and the electronics box as seen in Fig. 12. A breakdown of this mass is shown in Fig. 13.

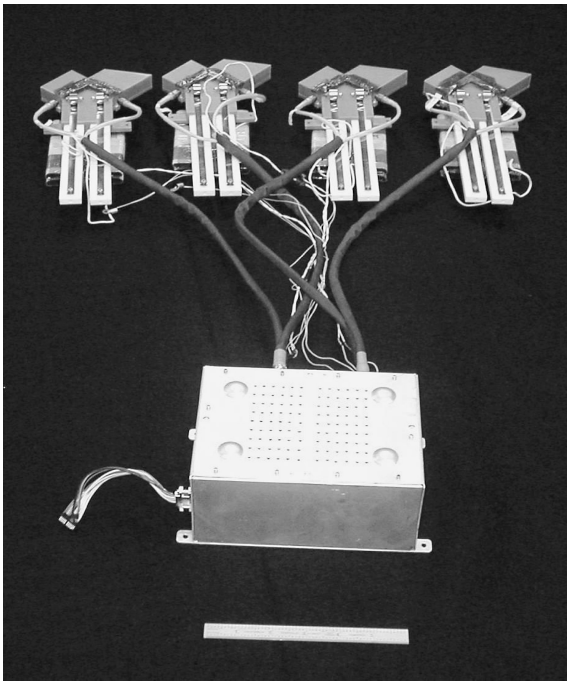

Fig. 12 Dawgstar flight pulsed plasma thruster system (note: 15-cm scale in foreground).

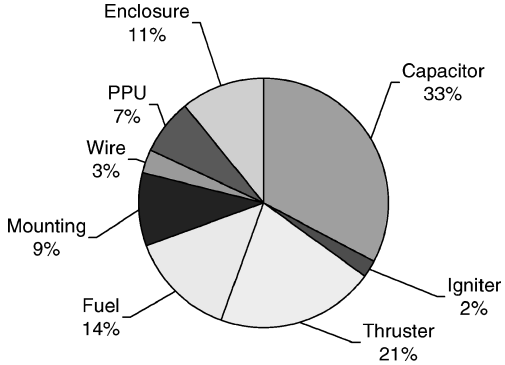

Fig. 13 Mass breakdown of the 4.20-kg Dawgstar pulsed plasma thruster system.

Conclusions

Extensive testing has provided proof that pulsed plasma thrusters are feasible within the limitations of micro- and nanosatellites. Specifically, a system was developed for the Dawgstar nanosatellite that has a total of eight thrusters and associated electronics for a mass of 4.2 kg. This system, shown in Fig. 12, can maintain satellite attitude with as little as 3.3-W orbit averaged power (based on a 375-km altitude orbit). In the event of thrust maneuvers and

formation flying, the system can fire two thrusters at a rate of up to 2 Hz each.

Capacitor testing identified mica-paper/foil as the most feasible capacitor technology for low-power pulsed plasma thrusters. This was because not only of high-energy density, but also because of the robustness of the capacitor itself. Initial impulse bit and specific impulse data show that the thruster operated as designed. Data also showed agreement with theory and thrusters of similar design. Extensive testing showed that arcing between electrodes is a significant hurdle in miniature PPT design. In the final configuration, materials with high dielectric strengths, separated strip lines, and labyrinths were utilized to prevent excessive carbon deposition. When the use of these features was incorporated into theory and modeled, their effect on overall performance was found to be insignificant. In parallel, significant improvements in circuit design utilizing high-voltage switching have resulted in improved electronics efficiency with a reduction in the overall mass when compared to previous designs.

Acknowledgments

This work was supported by a joint Washington Technology Center/Primex Space Systems (now Aerojet-Redmond Operations) grant. The Dawgstar satellite is supported by DARPA, U.S. Air Force Office of Scientific Research, Air Force Research Laboratory, and NASA. The authors acknowledge the assistance of W. Andrew Hoskins and Joe Cassady of Aerojet-Redmond Operations Operations for their expert guidance and support through the entire development process. The authors also thank Eric Pencil, Lynn Arrington, and Charles Sarmiento of NASA Glenn Research Center for their assistance with performance and EMI testing and to John Frus of Unison Industries for providing experimental capacitors and igniters for the development tests, as well as flight units for the Dawgstar flight thrusters.

References

[1]Spanjers, G., Bromaghim, D., Lake, J., Dulligan, M., White, D., Schilling, J., and Bushman, S., "AFRL MicroPPT Development for the TechSat 21 Flight," Vol. 1, Electric Rocket Propulsion Society, IEPC-01-166, Fairview Park, OH, 2001.

[2]Das, A., Cobb, R., and Stallard, M., "TechSat21—A Revolutionary Concept in Distributed Space Based Sensing," AIAA Paper 98-5255, Sept. 1998.

[3]Capps, R. W. (ed.), "Recommendations for Technology Development and Validation Activities in Support of the Origins Program," NASA-CR-203426, June 1996.

[4]Matossian, M. G., "A Teledesic Space Infrastructure Overview," *Proceedings, Mission Design and Implementation of Satellite Constellations*, edited by J. C. van der Ha, Vol. 1, Kluwer Academic, Dordrecht, The Netherlands, 1997, pp. 153–156.

[5]Zhurin, V. V., Porotnikov, A. A., and Shadov, V. P., "Electric Propulsion Research and Development in the USSR," AIAA Paper 76-1073, Nov. 1976.

[6]Vondra, R. J., "The MIT Lincoln Laboratory Pulsed Plasma Thruster," AIAA Paper 76-998, Nov. 1976.

[7]Ebert, W. L., Kowal, S. J., and Sloan, R. F., "Operational Nova Spacecraft Teflon Pulsed Plasma Thruster System," AIAA Paper 89-2497, July 1989; also AIAA A89-46876.

[8]Burton, R. L., and Turchi, P. J., "Pulsed Plasma Thruster," *Journal of Propulsion and Power*, Vol. 14, No. 5, 1998, pp. 718–735.

[9]Benson, S. W., Arrington, L. A., Hoskins, W. A., and Meckel, N. J., "Development of a PPT for the EO-1 Spacecraft," AIAA Paper 99-2276, June 1999.

[10]Zakrzwski, C., Davis, M., and Sarmiento, C., "Adressing EO-1 Spacecraft Pulsed Plasma Thruster EMI Concerns," AIAA Paper 2001-3641, July 2001.

[11]Zakrzwski, C., Benson, S., Sanneman, P., and Hoskins, W. A., "On-Orbit Testing of the EO-1 Pulsed Plasma Thruster," AIAA Paper 2002-3979, July 2002.

[12]Spanjers, G., Bromaghum, J., Lake, J., and Dulligan, M., "AFRL Micro-PPT Development for Small Spacecraft Propulsion," AIAA Paper 2002-3974, July 2002.

[13]Spores, R. A., Spanjers, G. G., Birkan, M., and Lawrence, T. J., "Overview of the USAF Electric Propulsion Program," AIAA Paper 2001-3225, July 2001.

[14]Bushman, S. S., "Investigations of Coaxial Pulsed Plasma Thruster," M.S. Thesis, Univ. of Illinois, Urbana, IL, 1999.

[15]Rysanek, F., and Burton, R. L., "Effects of Geometry on a Coaxial Pulsed Plasma Thruster," AIAA Paper 2000-3429, July 2000.

[16]Campbell, M., and Schetter, T., "Formation Flying Mission for the UW Dawgstar Nanosatellite," *Proceedings of the 2000 IEEE Aerospace Conference*, Vol. 1, Inst. of Electrical and Electronics Engineers Press, Piscataway, NJ, 2000.

[17]Swenson, C., and Fejer, B., "The Ionospheric Nanosatellite Formation, Exploring Space Weather," *Proceedings of the AIAA/USU Conference on Small Satellites*, Vol. 1, Utah State Univ. Press, Logan, UT, 2002.

[18]Luu, K., Martin, M., Stallard, M., Schlossberg, H., Mitola, J., Weidow, D., Blomquist, R., Campbell, M., Hall, C., Hansen, E., Horan, S., Kitts, C., Redd, F., Reed, H., Spence, H., and Twiggs, B., "University Nanosatellite Distributed Satellite Capabilities to Support TechSat 21," *Proceedings of the AIAA/USU Conference on Small Satellites*, Utah State Univ. Press, Logan, UT, 1999.

[19]Campbell, M., "Planning Algorithm for Large Satellite Clusters," AIAA Paper 2002-4958, Aug. 2002.

[20]Campbell, M., Knagenhjelm, V., and Yingling, J., "Flight Software Development for the ION-F Formation Flying Mission," *Proceedings of the 2001 IEEE Aerospace Conference*, Vol. 1, Inst. of Electrical and Electronics Engineers Press, Piscataway, NJ, 2001.

[21]Hoskins, W. A., Wilson, M. J., Willey, M. J., Meckel, N. J., Campbell, M. E., and Chung, S., "PPT Development Efforts at Primex Aerospace Company," AIAA Paper 99-2291, May 1999.

[22]Guman, W. J., "Pulsed Plasma Technology in Microthrusters," Fairchild Hiller Corp., AFARL-TR-132, Farmingdale, NY, Nov. 1968.

[23]Yuan-Zhu, K., "Effects of Propellant Geometry on PPT Performance," AIAA Paper 84-94, May 1994.

[24]Palumbo, D. J., and Guman, W. J., "Effects of Propellant and Electrode Geometry on Pulsed Ablative Thruster Performance," *Journal of Spacecraft and Rockets*, Vol. 13, No. 3, 1976, pp. 163–167.

[25]Haag, T. W., "PPT Thrust Stand," AIAA Paper 95-2917, July 1995.

[26]Haag, T. W., "Thrust Stand for Pulsed Plasma Thrusters," *Review of Scientific Instruments*, Vol. 68, No. 5, 1997, pp. 2060–2067.

[27]Hoskins, W. A., Rayburn, C. D., and Sarmiento, C., "Pulsed Plasma Thruster Electromagnetic Compatibility: History, Theory and the Flight Validation On EO-1," AIAA Paper 2003-5016, July 2003.

[28]Antropov, N., Gomilka, L., Diakonov, G., Krivonosov, I., Popov, G., and Orlov, M., "Parameters of Plasmoids Injected by PPT," AIAA Paper 97-2921, July 1997.

[29]Burton, T. A., Parker, K., and Sumlak, U., "Exhaust Plume Characterization of a Mini-PPT Using Time-of-Flight/Gridded Energy Analyzer," AIAA Paper 2002-4122, July 2002.

[30]Shumlak, U., Burton, T., and Parker, K., "Mass Characterization Measurements of a Mini-PPT Exhaust Plasma," AIAA Paper 2003-5169, July 2003.

I. D. Boyd
Associate Editor